MODELING OF DUST DEVIL ON MARS AND FLIGHT SIMULATION OF MARS AIRPLANE

Hirotaka Hiraguri*, Hiroshi Tokutake*
*Kanazawa University, Japan
hiraguri@stu.kanazawa-u.ac.jp;tokutake@se.kanazawa-u.ac.jp

Keywords: *Mars airplane, Flight control, Wind estimation, Gust avoidance, Soaring*

Abstract

A method for observing the winds on Mars using an airplane is proposed. Gusts such as dust storms and dust devils are known to occur frequently on Mars [1][2]. The highest known wind velocity for a dust devil is more than 100 m/s [1]. The atmosphere of Mars is considered to exhibit strong turbulence. Knowledge of the winds on Mars is important for future manned exploration and for design and control of airplanes to operate on Mars. We propose a flight profile and analysis method for use in obtaining statistical information about the winds on Mars. We show in this paper that the power spectral density of the wind with respect to the spatial frequency and time frequency can be constructed from the observed data. A guidance and control system for use in gust avoidance and soaring flight was also constructed in this study.

Nomenclature

C	Autocorrelation function
Δt	Sampling time
δ_a	Angle of aileron
δ_e	Angle of elevator
δ_r	Angle of rudder
$E(\Phi, \Theta, \Psi)$	Direction cosine matrix
G_s	Gradient of wind with respect to space
G_t	Gradient of wind with respect to time
H	Height of dust devil
K_P, K_Q, K_R	Control gains of roll, pitch, and yaw rates, respectively
K_{Pc}, K_{Qc}, K_{Rc}	Guidance gains of roll, pitch, and yaw rates commands, respectively
Ψ	Yaw angle
λ	Spatial frequency
ω	Time frequency
n	Sample number
P	Roll rate of airplane
Q	Pitch rate of airplane
R	Yaw rate of airplane
P_c	Roll rate command
Q_c	Pitch rate command
R_c	Yow rate command
R_d	Radius of dust devil
r	Position vector of airplane
S	Power spectral density
s	The local position along the path
t	time
U_r	Radial-direction velocity of dust devil
U_θ	Rotation-direction velocity of dust devil
U_h	Vertical-direction velocity of dust devil
V	Relative velocity of airplane with respect to ground
W	Wind velocity
W_a	Relative velocity of airplane with respect to wind
W_o	Wind velocity observed by airplane
x, y, z	Position of airplane
Φ	Roll angle of airplane
Θ	Pitch angle of airplane

Superscripts

b	Body-fixed frame
E	Ground-fixed frame

Subscript

x	x axis of rectangular coordinates
y	y axis of rectangular coordinates
z	z axis of rectangular coordinates

1 Introduction

A research group from Japan is considering a Mars exploration project using an airplane. A number of technical problems are involved, such as the development of available guidance, navigation, and control systems on Mars in the absence of global positioning system (GPS) satellites. The airplane for Mars exploration should be designed to be small and lightweight to satisfy strict constraints.

Previous Mars exploration revealed the existence of wind gusts on Mars that were observed from the ground and orbit. In addition to isolated climate phenomena such as dust devils, convection on Mars generates turbulence continuously [3]. These strong gusts could disrupt airplane dynamics and result in an airplane mission on Mars ending in failure. However, the characteristics of the winds on Mars have not been investigated precisely. Information about the winds on Mars is necessary for the success of an airplane observation mission and future manned exploration.

A research group from the National Aeronautics and Space Administration (NASA) also considered a Mars exploration project involving an airplane [4]. They reported the results of flight tests in regions with low Reynolds numbers [4]. However, to the best of our knowledge, there have been no reports to date of the use of flight control to address problems related to wind gusts on Mars.

Therefore, we focused in this study on a wind observation mission using an airplane. A flight profile that would make it possible to obtain statistical data on the winds on Mars is proposed in this paper. It is assumed that the velocity of the wind can be measured using an air data system, disturbance observer, and positioning system based on visual images. In addition, a guidance method for avoiding strong gusts is proposed. Gust avoidance can be accomplished using the estimated gradient of the wind velocity. This technique can be applied to soaring to extend the range of flight.

2 Wind estimation

2.1 Wind field

The wind velocity is assumed to be a function of the position and the time [5].

$$W^E(x,y,z,t) = \begin{bmatrix} W_x^E(x,y,z,t) \\ W_y^E(x,y,z,t) \\ W_z^E(x,y,z,t) \end{bmatrix} \quad (1)$$

The airplane's velocity vector is as follows.

$$V^E(t) = \begin{bmatrix} V_x^E(t) \\ V_y^E(t) \\ V_z^E(t) \end{bmatrix} \quad (2)$$

The wind velocity vector, W_a^E, that is observed directly by the airplane is defined as follows. Here, the airplane velocity is assumed to be constant.

$$W_a^E(x,y,z,t) = \begin{bmatrix} W_{ax}^E(x,y,z,t) \\ W_{ax}^E(x,y,z,t) \\ W_{ax}^E(x,y,z,t) \end{bmatrix}$$
$$= V^E(t) - W^E(x,y,z,t) \quad (3)$$

W_a^E is the relative velocity of the airplane with respect to the wind. Differentiating Eq. (3) with respect to time,

$$\frac{\mathrm{d}}{\mathrm{dt}} \begin{bmatrix} W_{ax}^E(x,y,z,t) \\ W_{ax}^E(x,y,z,t) \\ W_{ax}^E(x,y,z,t) \end{bmatrix}$$
$$= - \begin{bmatrix} \nabla W_x^E(x,y,z,t) \cdot V^E(t) \\ \nabla W_y^E(x,y,z,t) \cdot V^E(t) \\ \nabla W_z^E(x,y,z,t) \cdot V^E(t) \end{bmatrix}$$
$$- \begin{bmatrix} \frac{\partial}{\partial t} W_x^E(x,y,z,t) \\ \frac{\partial}{\partial t} W_y^E(x,y,z,t) \\ \frac{\partial}{\partial t} W_z^E(x,y,z,t) \end{bmatrix} \quad (4)$$

is obtained.
Equation (4) is expressed as follows:

$$G_t(x, y, z, t) = \begin{bmatrix} \dfrac{\partial}{\partial t} W_x^E(x, y, z, t) \\ \dfrac{\partial}{\partial t} W_y^E(x, y, z, t) \\ \dfrac{\partial}{\partial t} W_z^E(x, y, z, t) \end{bmatrix} \quad (5.1)$$

$$G_s(x, y, z, t) = \begin{bmatrix} \dfrac{\partial W_x^E}{\partial x} & \dfrac{\partial W_x^E}{\partial y} & \dfrac{\partial W_x^E}{\partial z} \\ \dfrac{\partial W_y^E}{\partial x} & \dfrac{\partial W_y^E}{\partial y} & \dfrac{\partial W_y^E}{\partial z} \\ \dfrac{\partial W_z^E}{\partial x} & \dfrac{\partial W_z^E}{\partial y} & \dfrac{\partial W_z^E}{\partial z} \end{bmatrix} \quad (5.2)$$

$$-\frac{d}{dt} W_a^E(x, y, z, t) = G_s(x, y, z, t) \cdot V^E(t)$$
$$+ G_t(x, y, z, t) \quad (5.3)$$

2.2 Wind velocity vector estimation methods

Table 1 lists the possible implemented sensors on the Mars airplane and the measured values.

Table 1 Sensors used for estimation methods

Sensors	Measured values
Positioning system	$x, y, z, V_x^E, V_y^E, V_z^E$
ADS	$W_{ax}^b, W_{ay}^b, W_{az}^b$
INS	Φ, Θ, Ψ
IMU	P, Q, R

A positioning system estimates the global position of an object based on visual images. An ADS (air data system) measures the relative velocity of an airplane with respect to the atmosphere based on the body-fixed axis. An INS (inertial navigation system) estimates the attitude of the airplane from the inertial sensor's outputs. An IMU (inertial measurement unit) outputs an angular velocity. Using these sensors' outputs, the wind velocity with respect to the ground can be calculated and analyzed. The methods for estimating the wind velocity are described below.

Method 1

A positioning system and ADS are used. The wind velocity with respect to the ground, W^E, can be calculated as the difference between the ground velocity of the airplane, V^E, and the airspeed of the airplane, W_a^E.

$$W^E(x, y, z, t) = V^E(t) - W_a^E(x, y, z, t) \quad (6)$$

The ground velocity of the airplane can be estimated from the positioning system. The airspeed of the airplane, expressed with respect to the ground-fixed axis, can be obtained from the ADS and INS.

$$W_a^E(x, y, z, t)$$
$$= E(\Phi, \Theta, \Psi)^{-1} W_a^b(x, y, z, t) \quad (7)$$

Here, W_a^b is the airspeed based on the body-fixed axis, which can be obtained from the ADS, and $E(\Phi, \Theta, \Psi)$ is the direction cosine matrix.

$$E(\Phi, \Theta, \Psi) = \begin{bmatrix} cos\Theta cos\Psi \\ sin\Phi sin\Theta cos\Psi - cos\Phi sin\Psi \\ cos\Phi sin\Theta cos\Psi + sin\Phi sin\Psi \end{bmatrix}$$
$$\begin{matrix} cos\Theta sin\Psi \\ sin\Phi sin\Theta sin\Psi + cos\Phi cos\Psi \\ cos\Phi sin\Theta sin\Psi - sin\Phi cos\Psi \end{matrix}$$
$$\begin{matrix} -sin\Theta \\ sin\Phi cos\Theta \\ cos\Phi cos\Theta \end{matrix} \Bigg] \quad (8)$$

Method 2

A GPS, ADS, and INS are used for this method. The observer is designed for an extended system that is constructed from the airplane dynamics and disturbance model. The velocity of the wind relative to the airplane velocity is estimated by the observer. Therefore, a positioning system is necessary to obtain the wind velocity with respect to the ground.

Method 3

The time derivatives of the wind velocity with respect to the ground are estimated based on the observer. If the airplane velocity is constant, the positioning system is not necessary.

These observer-based methods have the advantage that the dynamics model of the airplane can be introduced into the estimation.

In addition, the IMU outputs can be combined with the observer. Because more information can be used with this method than with method 1, it is possible to obtain more precise wind velocity estimates.

Table 2 lists estimated values and the sensor used. In an actual mission, combining these methods would increase the precision of the estimation.

Table 2 Estimated values and sensors used

	Method 1	Method 2	Method 3
Estimated value	W^E	W^E	$\dot{W}^E$
Positioning system	necessary	necessary	un necessary
ADS	necessary	necessary	necessary
INS	necessary	necessary	necessary
IMU	un necessary	necessary	necessary

2.3 Information acquired from estimation method

Determination of precise wind velocity data along the flight path by the wind observation mission is desirable. In addition, statistical information is required to understand the wind field on Mars. This information can be applied to airplane design and flight simulation for a future Mars mission.

The distribution of wind is a function of position and time. An airplane detects the wind only along its flight path. It is difficult to analyze characteristics that depend on the position and the time separately. For an airplane on Earth, because the velocity of an airplane is much greater than the time variant of the wind, a time-invariant wind model, such as the Dryden turbulence model [6], is typically used. However, we have a little information about the turbulence on Mars. Therefore, to obtain significant data from a mission using an airplane, the flight profile should be determined carefully based on the analysis method used.

The distribution of wind is assumed to be separable into a steady wind, $W_1^E(x, y, z)$, and a time-variant wind disturbance, $W_2^E(x, y, z, t)$. The steady wind is determined by the position.

The time-variant disturbance is determined by the position and the time.

$$W^E(x, y, z, t) = W_1^E(x, y, z) + W_2^E(x, y, z, t) \quad (9)$$

Here, the flight path, $\mathcal{P}$, is defined.

$$\mathcal{P} = \{(x, y, z) | (x, y, z) = \boldsymbol{r}(t) = \boldsymbol{b} + \boldsymbol{a}t\} \quad (10)$$

The wind velocity with respect to the ground that is observed by the airplane along the flight path becomes the following:

$$W_O^E(t) = W_1^E(\boldsymbol{r}(t)) + W_2^E(\boldsymbol{r}(t), t) \quad (11)$$

$W_O^E(t)$ can be estimated using the proposed estimation method described in section 2.2.

Let the autocorrelation functions of $W_1^E(x, y, z)$ about the x, y, and z axes and flight path s be $C_{W_{1x}^E}(\lambda)$, $C_{W_{1y}^E}(\lambda)$, $C_{W_{1z}^E}(\lambda)$, and $C_{W_{1r}^E}(\lambda)$, respectively.

$$C_{W_{1x}^E}(\lambda) = \lim_{X \to \infty} \frac{1}{X} \int_{-X}^{X} W_1^E(x, y, z)$$
$$\times W_1^E(x + \lambda, y, z) dx \quad (12)$$

$$C_{W_{1y}^E}(\lambda) = \lim_{Y \to \infty} \frac{1}{Y} \int_{-Y}^{Y} W_1^E(x, y, z)$$
$$\times W_1^E(x, y + \lambda, z) dy \quad (13)$$

$$C_{W_{1z}^E}(\lambda) = \lim_{Z \to \infty} \frac{1}{Z} \int_{-Z}^{Z} W_1^E(x, y, z)$$
$$\times W_1^E(x, y, z + \lambda) dz \quad (14)$$

$$C_{W_{1r}^E}(\lambda) = \lim_{L \to \infty} \frac{1}{L} \int_{-L}^{L} W_1^E(\boldsymbol{r}(t))$$
$$\times W_1^E\left(\boldsymbol{r}(t) + {}^{\boldsymbol{a}}\!/_{|\boldsymbol{a}|} \lambda\right) ds \quad (15)$$

Let the autocorrelation function of $W_2^E(x, y, z)$ about t be $C_{W_{2t}^E}(\tau)$.

$$C_{W_{2t}^E}(\tau) = \lim_{T \to \infty} \frac{1}{T} \int_{-T}^{T} W_2^E(x, y, z, t)$$
$$\times W_2^E(x, y, z, t + \tau) dt \quad (16)$$

It is assumed that $W_1^E(x, y, z)$ is isotropic:

$$C_{W_{1x}^E}(\lambda) = C_{W_{1y}^E}(\lambda) = C_{W_{1z}^E}(\lambda) = C_{W_{1r}^E}(\lambda) \quad (17)$$

The time-variant wind disturbance, $W_2^E(x, y, z, t)$, is assumed to be a stationary process.

$$\forall \boldsymbol{r}, \lim_{T \to \infty} \frac{1}{T} \int_{-T}^{T} W_2^E(\boldsymbol{r}, t) W_2^E(\boldsymbol{r}, t + \tau) dt$$
$$= const \quad (18)$$

Without loss of generality, the time-averaged wind disturbance, $W_2^E(x, y, z, t)$, is assumed to be 0.

$$\forall r, \lim_{T \to \infty} \frac{1}{T} \int_{-T}^{T} W_2^E(r, t)\, dt = 0 \qquad (19)$$

The cross-correlation between W_1^E and W_2^E is assumed to be zero.

$$\lim_{T \to \infty} \frac{1}{T} \int_{-T}^{T} W_1^E(r(t))\, W_2^E(r(t+\tau), t+\tau)\, dt$$
$$= \lim_{T \to \infty} \frac{1}{T} \int_{-T}^{T} W_1^E(r(t+\tau))\, W_2^E(r(t), t)\, dt$$
$$= 0 \qquad (20)$$

The autocorrelation function of the observed wind data, W_O^E, about t becomes the following:

$$C_{W_O^E}(\tau)$$
$$= \lim_{T \to \infty} \frac{1}{T} \int_{-T}^{T} \Big(W_1^E(r(t)) + W_2^E(r(t), t) \Big)$$
$$\times \Big(W_1^E(r(t+\tau)) + W_2^E(r(t+\tau), t+\tau) \Big) dt$$
$$= \lim_{T \to \infty} \frac{1}{T} \int_{-T}^{T} W_1^E(r(t))\, W_1^E(r(t+\tau))\, dt$$
$$+ \lim_{T \to \infty} \frac{1}{T} \int_{-T}^{T} W_1^E(r(t))\, W_2^E(r(t+\tau), t+\tau)\, dt$$
$$+ \lim_{T \to \infty} \frac{1}{T} \int_{-T}^{T} W_2^E(r(t+\tau), t)\, W_1^E(r(t+\tau))\, dt$$
$$+ \lim_{T \to \infty} \frac{1}{T} \int_{-T}^{T} W_2^E(r(t), t)$$
$$\times W_2^E(r(t+\tau), t+\tau)\, dt \qquad (21)$$

From Eqs. (18), and (20), Eq. (21) becomes the following:

$$C_{W_O^E}(\tau)$$
$$= \lim_{T \to \infty} \frac{1}{T} \int_{-\frac{1}{T}}^{\frac{1}{T}} W_1^E(r(t))\, W_1^E(r(t+\tau))\, dt$$
$$+ \lim_{T \to \infty} \frac{1}{T} \int_{-\frac{1}{T}}^{\frac{1}{T}} W_2^E(r(t), t)$$
$$\times W_2^E(r(t+\tau), t+\tau)\, dt \qquad (22)$$

The airplane is assumed to be flying at a constant velocity, $|r'|$, when the wind velocity is observed.

$$|r'| = \frac{ds(t)}{dt} = const \qquad (23)$$

From Eqs. (22) and (23), the following equation is obtained.

$$C_{W_O^E}(\tau) = \frac{1}{|r'|} \lim_{L \to \infty} \frac{1}{L} \int_{-L}^{L} W_1^E(r(t))$$
$$\times W_1^E(r(t) + |r'|\tau)\, ds$$
$$+ \lim_{T \to \infty} \frac{1}{T} \int_{-T}^{T} W_2^E(r(t), t)$$
$$\times W_2^E(r(t+\tau), t+\tau)\, dt$$
$$= \frac{1}{|r'|} C_{W_{1r}^E}(|r'|\tau) + C_{W_{2t}^E}(\tau) \qquad (24)$$

When $\tau = 0$,

$$\sigma^2(W_O^E) = \frac{1}{|r'|} \sigma^2(W_{1r}^E) + \sigma^2(W_{2t}^E) \qquad (25)$$

is satisfied.

The power spectral density of W_1^E with respect to space and the power spectral density of W_2^E with respect to time are as follows:

$$S_{W_{1r}^E}(\lambda) = \int_{-\infty}^{\infty} C_{W_{1r}^E}(s)\, e^{-j\lambda s}\, ds \qquad (26)$$

$$S_{W_{2t}^E}(\omega) = \int_{-\infty}^{\infty} C_{W_{2t}^E}(t)\, e^{-j\omega t}\, dt \qquad (27)$$

The power spectral density of $W_O^E(t)$ becomes the following:

$$S_{W_O^E}(\omega) = \int_{-\infty}^{\infty} C_{W_O^E}(\tau)\, e^{-j\omega \tau}\, d\tau$$
$$= \frac{1}{|r'|} \int_{-\infty}^{\infty} C_{W_{1r}^E}(|r'|\tau)\, e^{-j\omega \tau}\, d\tau$$
$$+ \int_{-\infty}^{\infty} C_{W_{2t}^E}(\tau)\, e^{-j\omega \tau}\, d\tau$$
$$= \frac{1}{|r'|^2} \int_{-\infty}^{\infty} C_{W_{1r}^E}(\tau')\, e^{-j\frac{\omega}{|r'|}\tau'}\, d\tau'$$
$$+ \int_{-\infty}^{\infty} C_{W_{2t}^E}(\tau)\, e^{-j\omega \tau}\, d\tau$$
$$= \frac{1}{|r'|^2} S_{W_{1r}^E}\left(\frac{\omega}{|r'|}\right) + S_{W_{2t}^E}(\omega) \qquad (28)$$

where $|r'|\tau = \tau'$.

Because $W_O^E(t)$ is the wind velocity along the flight path, it can be observed directly and is available for analysis. However, the statistical value depends on the flight velocity, as shown in Eq. (25). Therefore, we propose a flight profile that permits statistical analysis using the data measured directly along the flight path.

The flight profile is designed to have at least two steady flight paths with different constant velocity, as shown below:

$$\begin{aligned}
\mathcal{P}_1 = \{(x,y,z)|(x,y,z) \\
= r_1(t), ds_1/dt = |r'_1| \\
= const\} \quad (29)
\end{aligned}$$

$$\begin{aligned}
\mathcal{P}_2 = \{(x,y,z)|(x,y,z) \\
= r_2(t), ds_2/dt = |r'_2| \\
= const\} \quad (30)
\end{aligned}$$

The observed wind velocities along the flight paths are as follows:

$$W_{O_1}^E(t) = W_1^E(r_1(t)) + W_2^E(r_1(t), t) \quad (31)$$

$$W_{O_2}^E(t) = W_1^E(r_2(t)) + W_2^E(r_2(t), t) \quad (32)$$

Let $\sigma^2(*)$ be the variance of $*$. From Eq. (25), the following variance equations are obtained:

$$\sigma^2(W_{O_1}^E) = \frac{1}{|r'_1|}\sigma^2(W_{1_r}^E) + \sigma^2(W_{2_t}^E) \quad (33)$$

$$\sigma^2(W_{O_2}^E) = \frac{1}{|r'_2|}\sigma^2(W_{1_r}^E) + \sigma^2(W_{2_t}^E) \quad (34)$$

These equations result in the following:

$$\sigma^2(W_{1_r}^E) = \frac{|r'_1||r'_2|}{|r'_2| - |r'_1|} \\
\times \left(\sigma^2(W_{O_1}^E) - \sigma^2(W_{O_2}^E)\right)$$

$$\sigma^2(W_{2_t}^E) = \\
\frac{|r'_2|\sigma^2(W_{O_2}^E) - |r'_1|\sigma^2(W_{O_1}^E)}{|r'_2| - |r'_1|} \quad (35)$$

It is clear that the variance of the wind distribution model can be estimated from the observed wind data along the proposed flight profile.

Next, the power spectral density is constructed from the observed data. Let $S_{W_{O_1}^E}(\omega)$ and $S_{W_{O_2}^E}(\omega)$ be the power spectral densities of the observed wind velocity along flight paths $\mathcal{P}_1$ and $\mathcal{P}_2$, respectively.

$$S_{W_{O_1}^E}(\omega) = \frac{1}{|r'_1|^2}S_{W_{1_r}^E}\left(\frac{\omega}{|r'_1|}\right) + S_{W_{2_t}^E}(\omega) \quad (36)$$

$$S_{W_{O_2}^E}(\omega) = \frac{1}{|r'_2|^2}S_{W_{1_r}^E}\left(\frac{\omega}{|r'_2|}\right) + S_{W_{2_t}^E}(\omega) \quad (37)$$

The left sides of Eqs. (36) and (37) can be calculated from the observed data.

From Eqs. (36) and (37),

$$S_{W_{O_1}^E}(\omega) - S_{W_{O_2}^E}(\omega)$$

$$= \frac{1}{|r'_1|^2}S_{W_{1_r}^E}\left(\frac{\omega}{|r'_1|}\right) - \frac{1}{|r'_2|^2}S_{W_{1_r}^E}\left(\frac{\omega}{|r'_2|}\right) \quad (38)$$

is satisfied. The power spectral densities of $S_{W_{O_1}^E}(\omega) - S_{W_{O_2}^E}(\omega)$ and $S_{W_{1_r}^E}(\lambda)$ are approximated as polynomial functions of frequency, as shown below:

$$S_{W_{O_1}^E}(\omega) - S_{W_{O_2}^E}(\omega) = \sum_{i=0}^{n} a_i\omega^i \quad (39)$$

$$S_{W_{1_r}^E}(\lambda) = \sum_{i=0}^{n} b_i\lambda^i \quad (40)$$

By substituting Eqs. (39) and (40) into Eq. (38), the following is satisfied.

$$\begin{aligned}
\sum_{i=0}^{n} a_i\omega^i &= \frac{1}{|r'_1|^2}\sum_{i=0}^{n} b_i\left(\frac{\omega}{|r'_1|}\right)^i \\
&\quad - \frac{1}{|r'_2|^2}\sum_{i=0}^{n} b_i\left(\frac{\omega}{|r'_2|}\right)^i \\
&= \sum_{i=0}^{n} b_i\left(\frac{1}{|r'_1|^{i+2}} - \frac{1}{|r'_2|^{i+2}}\right)\omega^i \quad (41)
\end{aligned}$$

Finally, the following equation is obtained.

$$b_i = \frac{a_i(|r'_1||r'_2|)^{i+2}}{(|r'_2|^{i+2} - |r'_1|^{i+2})} \quad (42)$$

Therefore, the power spectral density of W_1^E with respect to space becomes the following:

$$S_{W_{1_r}^E}(\lambda) = \sum_{i=0}^{n} \frac{a_i(|r'_1||r'_2|)^{i+2}}{(|r'_2|^{i+2} - |r'_1|^{i+2})}\lambda^i \quad (43)$$

As a result, the power spectral density of W_2^E with respect to time becomes the following:

$$S_{W_{2_t}^E}(\omega)$$

$$= S_{W_{O_1}^E}(\omega) - \sum_{i=0}^{n} \frac{a_i|r'_2|^{i+2}}{(|r'_2|^{i+2} - |r'_1|^{i+2})}\omega^i \quad (44)$$

$S_{W_{O_1}^E}(\omega)$ and $S_{W_{O_2}^E}(\omega)$ can be calculated from the observed data. Using Eqs. (43) and (44), the power spectral densities of the time-variant and time-invariant components of the wind model can be constructed. This analysis is possible when the airplane flies along the proposed flight profile.

2.4 Model for dust devils on Mars

A model for a dust devil, a typical climate phenomenon on Mars, is presented in this section. The wind velocity distribution of a dust devil was modeled using data observed for Mars and Earth. The observed data for Mars were used to define the wind velocity, radius, and height of the dust devil. The observed data for Earth were used to define the structure of the wind velocity [1,7-9]. The modeled wind velocity distribution of the dust devil is shown in Fig. 1. The important characteristics of this model are as follows: the radial-direction velocity, U_r, is dominant outside the dust devil; the vertical-direction velocity, U_h, is dominant inside the dust devil; and the rotation-direction velocity, U_θ, is approximated by the Rankine vortex [1].
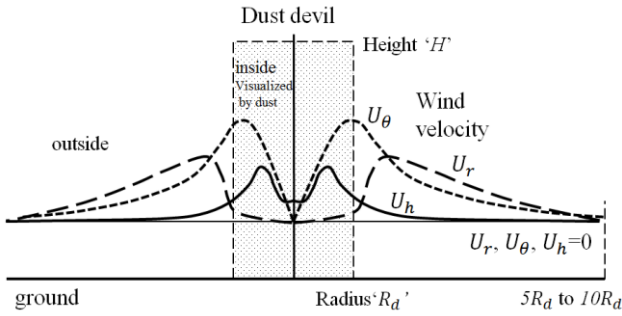
Fig. 1 Wind velocity distribution of dust devil[1]

The wind velocity distribution of a dust devil is shown as a function of the radius r and altitude h in equations (45)–(53).

$$U_r = a_r(h)\left(1 - \cos\left(\frac{2r\pi}{5R_d}\right)\right)$$
$$(0 \leq r < 2R_d)(45)$$

$$U_r = b_{r_4}(h)r^4 + b_{r_3}(h)r^3 + b_{r_2}(h)r^2 \\ + b_{r_1}(h)r + b_{r_0}(h)$$
$$(2R_d \leq r < 3R_d)(46)$$

$$U_r = \frac{c_r(h)}{r + d_r(h)} + c_{uo}(h)$$
$$(3R_d \leq r \leq 7R_d)(47)$$

$$U_\theta = a_{\theta 1}(h)r$$
$$\left(0 \leq r < \frac{3}{4}R_d\right)(48)$$

$$U_\theta = b_{\theta_4}(h)r^4 + b_{\theta_3}(h)r^3 \\ + b_{\theta_2}(h)r^2 + b_{\theta_1}(h)r + b_{\theta_0}(h)$$
$$\left(\frac{3}{4}R_d \leq r < \frac{5}{4}R_d\right)(49)$$

$$U_\theta = \frac{c_\theta(h)}{r + d_\theta(h)} + c_{\theta o}(h)$$
$$\left(\frac{5}{4}R_d \leq r \leq 7R_d\right)(50)$$

$$U_h = a_h(h)\left(1 - \cos\left(\frac{4r\pi}{3R_d}\right)\right)$$
$$\left(0 \leq r < \frac{3}{4}R_d\right)(51)$$

$$U_h = b_{h_4}(h)r^4 + b_{h_3}(h)r^3 \\ + b_{h_2}(h)r^2 + b_{h_1}(h)r + b_{h_0}(h)$$
$$\left(\frac{3}{4}R_d \leq r < \frac{5}{4}R_d\right)(52)$$

$$U_h = \frac{c_h(h)}{r + d_h(h)} + c_{ho}(h)$$
$$\left(\frac{5}{4}R_d \leq r \leq 7R_d\right)(53)$$

The coefficients of the dust devil model are determined from the size and maximum velocity of dust devils.
 In addition, the following relation is known to hold [1].

$$\sqrt{U_{rmax}^2 + U_{\theta max}^2} = 4U_{hmax} \qquad (54)$$

Table 3 describes the typical size of dust devils on Mars. [1][10]

Table 3 Size of dust devils on Mars

$2R_d$	45–1650 m mostly < 400 m
H	75–4440 m mostly < 1000 m
$\sqrt{U_{rmax}^2 + U_{\theta max}^2}$	~100 m/s mostly < 30 m/s

3 Application to guidance for gust avoidance

Strong gusts that could cause the failure of the mission may exist on Mars. The airplane should therefore be guided to avoid gusts. However, if the airplane is guided to enter the gust, sufficient data can be obtained. In addition, if the airplane is guided to the updraft, soaring can be performed. Therefore, a guidance method that uses estimated wind data is proposed.

If the wind velocity relative to the airplane velocity is constant, the airplane can easily maintain a steady flight. Variation in the wind is important to gust avoidance or flight entering gust. flight. The velocity of the airplane is assumed to be constant. In Eq. (5), it is assumed that $G_s = const$ and that the average of G_t over time is zero.

$$\lim_{T \to \infty} \frac{1}{T} \int_0^T G_t(x, y, z, t) dt = 0 \qquad (55)$$

$$-\frac{d}{dt} W_O^E(t) - G_t(x, y, z, t) = G_s \cdot V(t)^E \qquad (56)$$

From the measured data, the gradient of wind distribution is estimated and is provided to the guidance system. Let $\dot{W}^E{}_i$ and $V^E{}_i$ be the measured $\dot{W}^E$ and V^E, respectively, at the sampling time, t_i. Let G_{t_i} be G_t at the sampling time, t_i. The following data matrixes are constructed.

$$V_m{}^E = [V^E{}_0 \quad V^E{}_1 \quad \cdots \quad V^E{}_{n-1} \quad V^E{}_n] \quad (57.1)$$

$$\dot{W}^E{}_m = [\dot{W}^E{}_0 \quad \dot{W}^E{}_1 \quad \cdots \quad \dot{W}^E{}_{n-1} \quad \dot{W}^E{}_n] \quad (57.2)$$

$$G_{t_m} = [G_{t_0} \quad G_{t_1} \quad \cdots \quad G_{t_{n-1}} \quad G_{t_n}] \quad (57.3)$$

Eqs. (56) and (57) become the following:

$$-\dot{W}^E{}_m - G_{t_m} = G_s \cdot V_m{}^E \qquad (58)$$

The flight profile is determined to have at least three flight paths with independent constant-velocity vectors.

$$\text{rank}(V_m{}^E) = 3 \qquad (59)$$

Multiplying the pseudo-inverse matrix of $V_m{}^E$ from the right side of Eq. (58) yields the following:

$$G_s = -\dot{W}^E{}_m \cdot V_m{}^{E^+} - G_{t_m} \cdot V_m{}^{E^+} \qquad (60)$$

$G_{t_m} \cdot V_m{}^{E^+}$ is zero because the velocity of the airplane is constant and the average G_t over time is zero. According to Eq. (55), $G_{t_m} \cdot V_m{}^{E^+}$

becomes zero when the sampling number is large.

$$G_s \cong -\dot{W}^E{}_m \cdot V_m{}^{E^+} \qquad (61)$$

The gradient of the wind velocity, G_s, can be calculated from the measured data.
The estimated gradient of the airplane velocity is provided to the guidance controller, and an angular velocity command is generated. The error between the generated command and the measured angular velocity are input into the stabilizing controller (Fig. 2).
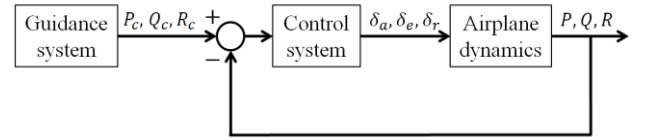

Fig. 2 Proposed system

$$G_{s_z}{}^E \triangleq \left[\frac{\partial W_z^E}{\partial x} \quad \frac{\partial W_z^E}{\partial y} \quad \frac{\partial W_z^E}{\partial z} \right] \qquad (62)$$

$$G_{s_z}{}^b = \left[G_{s_z}{}^b{}_x \quad G_{s_z}{}^b{}_y \quad G_{s_z}{}^b{}_z \right]^T$$
$$\triangleq E(\Phi, \Theta, \Psi) \cdot G_{s_z}{}^{E^T} \qquad (63)$$

$$P_C = K_{Pc} \times G_{s_z}{}^b{}_y \qquad (64)$$

$$Q_C = K_{Qc} \times G_{s_z}{}^b{}_z \qquad (65)$$

$$R_C = K_{Rc} \times G_{s_z}{}^b{}_y \qquad (66)$$

$$\delta_a = K_P(P_c - P) \qquad (67)$$

$$\delta_e = K_Q(Q_c - Q) \qquad (68)$$

$$\delta_r = K_R(R_c - R) \qquad (69)$$

The guidance gains K_{Pc}, K_{Qc}, and K_{Rc} should be determined appropriately. In particular, the sign of each guidance gain depends on the purpose of the guidance. For example, W_z^E is essential for soaring and avoidance of downbursts. These types of guidance are provided by increasing W_z^E. The absolute values $|W_x^E|$, $|W_y^E|$, and $|W_z^E|$ are essential for avoiding gust areas. This type of guidance is provided by decreasing $|W_x^E|$, $|W_y^E|$, and $|W_z^E|$.

4 Mars airplane model

Fig. 3 and Table 4 present the Mars airplane and its key design specifications. This airplane design is an example developed for the purpose of verification of the proposed method.

Table 4 Specifications of the Mars airplane design

Mass	5.610 kg
Wing span	2.404 m
Wing chord	0.49 m
Wing area	1.178 m^2

Table 5 lists the design conditions for steady turning.

Table 5 Assumed flight conditions of Mars airplane

Velocity along x^b axis	63.28 m/s
Velocity along y^b axis	0 m/s
Velocity along z^b axis	11.16 m/s
Angle of attack	10°
Pitch angle	-1.10°
Roll angle	20°
Density of atmosphere	0.01 kg/m^3
Gravity acceleration	3.72 m/s^2
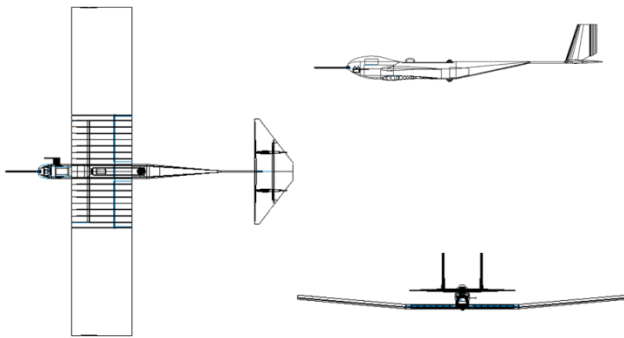
Fig. 3 Mars airplane

Using the results of wind tunnel testing, a nonlinear dynamic model of the Mars airplane was formulated. Because the inherent dynamics are unstable, a stabilizing controller was found to be necessary.

5 Simulations

The proposed gust avoidance method was validated by the simulation. A nonlinear six-degree-of-freedom model of the Mars airplane was used in the simulation. The parameters of the simulated dust devil are listed in Table 6.

Table 6 Parameters of dust devil used for simulation

R_d	215 m
H	2000 m
U_{rmax}	20 m/s
$U_{\theta max}$	30 m/s
U_{hmax}	10 m/s

The dust devil model generates a steady wind. During an actual flight, the airplane would experience time-variant turbulence. In the simulation, a gust factor was introduced to reflect time-variant turbulence. The gust factor is the ratio of the maximum velocity to the average velocity. On Earth, typical gust factors are in the range of 1.5 to 2. In the simulation, white noise was input as turbulence corresponding to a gust factor of 1.3.

In the simulation, it was assumed that the wind velocity could be detected by the airplane. The gradient of the wind velocity is calculated numerically from the airplane position data.

Table 7 lists the guidance and control gains used. These values were determined to avoid a dust devil with trial and error manner. The sample number was 20, and the sampling time was 0.005 s.

Figures 4–6 show the wind fields of the dust devil at an altitude of 1000 m.

Table 7 Guidance gains and control gains

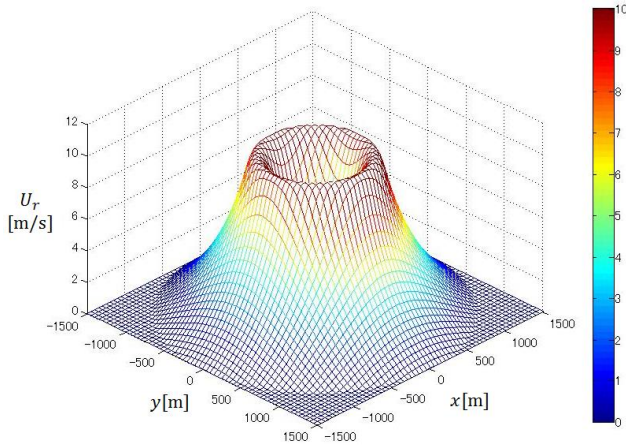| K_{Pc}	K_{Qc}	K_{Rc}	K_P	K_Q	K_R
0.05	0	0.05	-1	-1	3

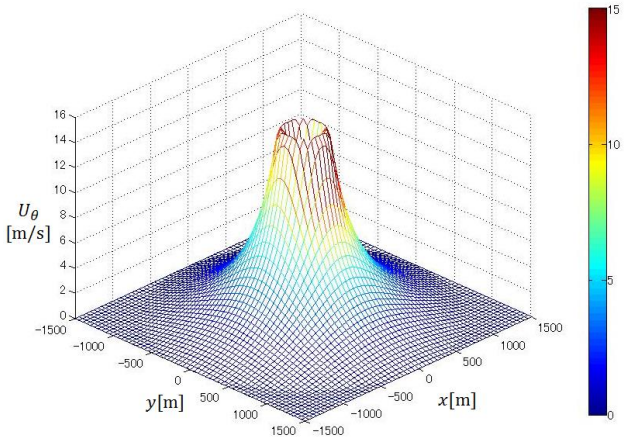Fig. 4 Wind field U_r of dust devil at an altitude of 1000 m

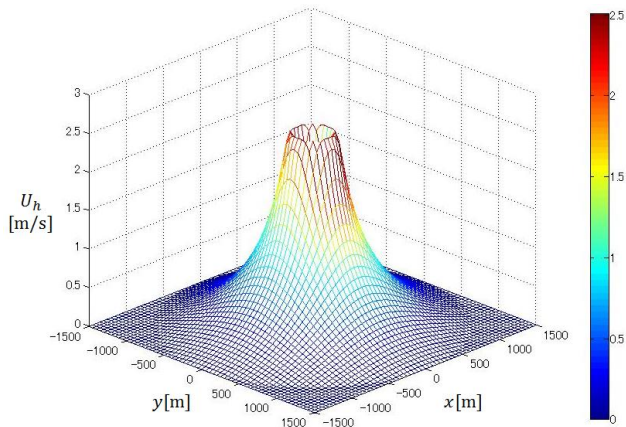Fig. 5 Wind field U_θ of dust devil at an altitude of 1000 m

Fig. 6 Wind field U_h of dust devil at an altitude of 1000 m
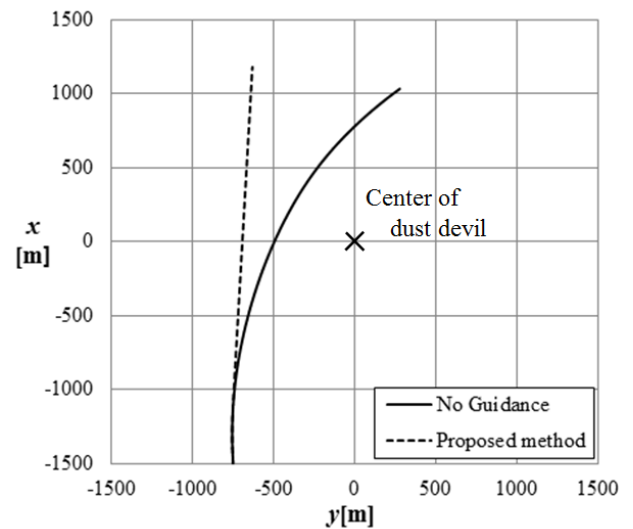
The simulation results are show in Figs. 7–9. The flight path without gust avoidance is shown in each figure for comparison.

The trimmed condition is a steady right turn. Therefore, the airplane approached to the dust devil without gust avoidance guidance (Figs. 7 and 8). As a result, the pitch dynamics were strongly disturbed (Fig. 9). However, the airplane was guided in the right direction to avoid approaching the dust devil using the proposed method. The pitch dynamics were not strongly disturbed (Fig. 9).

In this simulation, it was assumed that the wind velocity was detected directly. The precision of the detection depend on the performance of the sensors used and the characteristics of the actual wind. More realistic validation will be necessary before the mission can be finalized.
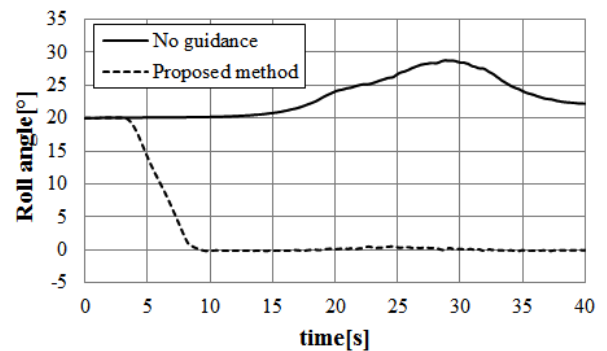

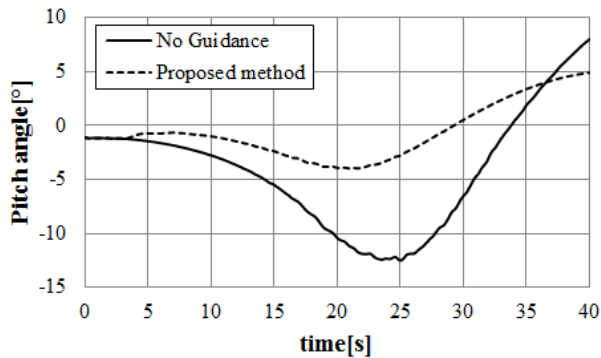Fig. 7 Position

Fig. 8 Roll angle

Fig. 9 Pitch angle

6 Conclusions

Methods for estimating the wind field on Mars and providing flight guidance for an airplane on Mars using wind velocity data are proposed in this paper. The wind field is a function of the position and the time. It is difficult to analyze wind data obtained along the flight path. Therefore, a flight profile that permits statistical analysis of the wind field is proposed. This method can be applied to in situ analysis to decrease the amount of data transmitted. In addition, this method makes it possible to perform online tuning of the flight controller in response to turbulence information.

 Because the wind field on Mars has not been investigated very well, gust avoidance technology is very important to completing a mission using an airplane. If soaring based on the estimated wind velocity is implemented, the flight duration and range can be extended and the success level of the mission can be increased.

Acknowledgements

References

[1] Thomas P., Gierasch P. J.: Dust devils on Mars. *Science*, vol. 230, pp. 175-177, 1985.

[2] Bruce A., Philip B., Caplinger M., Wolff, M. J.: Martian dust storms:1999 Mars Orbiter Camera observations. *Journal of Geophysical Research*, vol. 106, 23,653-23,687, 2001.

[3] Nishizawa et al.: High resolution large eddy simulation of the Martian planetary boundary layer, *Proceedings of the 46th ISAS Lunar and Planetary Symposium, 2014.*

[4] Lede J. C., Croom M. A., Parks R.: High Altitude Drop Testing in Mars Relevant Conditions for the ARES Mars Scout Mission. *AIAA Paper,* 2003-6609, 2003.

[5] Langelaan J. W., Alley N., Neidhoefer J.: Wind Field Estimation for Small Unmanned Aerial Vehicles. *AIAA paper* 2010-8177, 2010.

[6] McLean D.: *Automatic Flight Control Systems.* Prentice-Hall International, 1990.

[7] Rafkin S. C. R.: A positive radiative-dynamic feedback mechanism for the maintenance and growth of Martian dust storms. *Journal of Geophysical Research*, vol. 114, E01009, 2009.

[8] Balme M., Greeley R.: Dust devils on Earth and Mars. *Review of Geophysics*, vol. 44, RG3003, 2006.

[9] Ferri F., Smith P. H., Lemmon M., Renno N. O.: Dust devils as observed by Mars Pathfinder. *Journal of Geophysical Research*, vol. 108, 5133, 2003.

[10] Stanzel C., Pätzold M., Williams D. A., Whelley P. L., Greeley R., Neukum G.: Dust devil speeds, directions of motion and general characteristics observed by the Mars Express High Resolution Stereo Camera. *Icarus* 197, pp. 39-51, 2008.

Copyright Statement